Electronic Supplementary Information

Experimental Section

Materials: Copper nitrate trihydrate ($Cu(NO_3)_2·3H_2O$), ferric nitrate nonahydrate ($Fe(NO_3)_2·9H_2O$), N,N-Dimethylformamide (DMF), ammonium chloride (NH_4Cl), sulfuric acid (H_2SO_4), hydrochloric acid (HCl)，Cupric oxide (CuO) were purchased from Kelong chemical Ltd (Chengdu, China). Polyvinylpyrrolidone (PVP Mw = 1300000), polyacrylonitrile (PAN Mw=150000), sodium nitrate ($NaNO_3$)，sodium nitrite ($NaNO_2$), sodium nitroferricyanide dihydrate ($C_5FeN_6Na_2O·H_2O$), sodium salicylate ($C_7H_5NaO_3$), salicylic acid ($C_7H_6O_3$), trisodium citrate dihydrate ($C_6H_5Na_3O_7·2H_2O$), p-dimethylaminobenzaldehyde ($C_9H_{11}NO$), 0.8 wt% sulfamic acid solution (H_3NO_3S), sodium hypochlorite solution (NaClO), sodium dihydrogen phosphate dihydrate ($NaH_2PO_4·H_2O$) ，disodium phosphate (Na_2HPO_4) were bought from Aladdin Ltd (Shanghai, China). Nafion solution (5 wt%) came from Sigma-Aldrich Chemical Reagent Co., Ltd. Deionized water was purified through a Millipore system.

Preparation of $CuFe_2O_4$ and $CuO@CuFe_2O_4$: $CuFe_2O_4$ nanotubes was synthesized according to electrospinning. 0.5g PVP and 0.5g PAN were dissolved in 10 ml DMF with stirring for 1 h. Then 0.096 g $Cu(NO_3)_2·3H_2O$ and 0.323g $Fe(NO_3)_2·9H_2O$ were added into the above solution with stirring for 24 h at room temperature to form precursor solution.

During the spinning process, a high voltage of 18 kV was applied between the tip of a 10 mL syringe the grounding electrode and the aluminum foil collector placed at a distance of 10 cm, with the precursor fed at a rate of 0.8 mL h^{-1}. Annealing of the collected composite fibers. The fibers were firstly heated up to 200 °C at a 1 °C min^{-1} heating rate and held for one hour to allow the decomposition of the organic fraction

without altering the microstructure. Then, the samples were heated to 600 °C at a rate of 1°C min $^{-1}$ and kept 600 °C for 2h. Finally, they are cooled to room temperature at a rate of 1°C min $^{-1}$. As for CuO@$CuFe_2O_4$, 0.193 g $Cu(NO_3)_2 \cdot 3H_2O$ and 0.162 g $Fe(NO_3)_2 \cdot 9H_2O$ were added into the solution, and the fabrication process was the same as that for the $CuFe_2O_4$ nanotubes.

Here comes the reaction equation:

$$Fe^{2+} + 2OH^- \leftrightarrow Fe(OH)_{2(s)} \quad KSP = 4.87\times10^{-17} \tag{1}$$

$$Cu^{2+} + 2OH^- \leftrightarrow Cu(OH)_{2(s)} \quad KSP = 4.8\times10^{-20} \tag{2}$$

$$Cu(OH)_2 \rightarrow CuO + H_2O \tag{3}$$

$$Fe(OH)_2 \rightarrow FeO + H_2O \tag{4}$$

$$2FeO + \frac{1}{2} O_2 \rightarrow Fe_2O_3 \tag{5}$$

$$Fe_2O_3 + CuO \rightarrow CuFe_2O_4 \tag{6}$$

$$CuO + CuFe_2O_4 \rightarrow CuO@CuFe_2O_4 \tag{7}$$

Characterization: X-ray diffraction (XRD) analysis of the samples was performed using a LabX XRD-6100 X-ray diffractometer with Cu Kα radiation at 0.154 nm. Hitachi S-4800 scanning electron microscope (SEM) was used to observe the morphology and microstructure of the samples. The samples were observed using a JEOL JEM 2100F high resolution field emission transmission electron microscope (TEM) (the samples were dispersed over a copper grid). X-ray photoelectron spectroscopy (XPS) measurements were performed using an Al K ALPH source on Thermo Scientific K-Alpha X-ray Photoelectron spectrometer in a high-purity nitrogen atmosphere.

Electrochemical methods: Absorbance data are acquired from SHIMADZU UV-1800 uV-vis spectrophotometer. The concentrations of ammonium and nitrite are calculated from the standard concentration curve. Throughout all the measurement, a three-electrode system is utilized. Catalyst is deposited on the treated carbon paper and Nafion is used as the protective film. Carbon rod is employed as the counter electrode, and stable Ag/AgCl/KCl is used as the reference electrode. The neutral 0.1 M PBS

electrolyte is replaced when the voltage is changed. Ammonia production rate and Faraday efficiency are calculated using the following formulas:

$$NH_3(yield)=V\times[NH_3]/(m\times t)$$

$$FE=8F\times V\times[NH_3]/ (Q\times 17) \times 100\%$$

where V means the electrolytic liquid volume, Q the amount of reaction charge, m the mass of the catalyst.

Determination of NH_3: Indophenol blue method is adopted to quantify the concentration of produced NH_3. The electrolytes after 1 h electrolysis is diluted 20 times to 2 mL and then added 2 mL of coloring solution (1 M NaOH containing 5 wt% salicylic acid and 5 wt% sodium citrate), 1 mL of the oxidizing solution (0.05 M sodium hypochlorite solution) and 200 uL catalyst solution (1 wt% sodium nitroferricyanide (III) dehydrate) one by one. After the mixed solution reacts for 2 h in the dark, the UV-Vis absorption spectra are performed at λ = 665 nm. We calibrate the standard NH_4Cl solutions with different concentration and then calculate the fitting curve (y=0.449x +0.0336, R^2=0.999).

Determination of NO_2^-: The electrolytes after 1 h electrolysis is diluted 20 times to 1 mL and 1 mL color reagent (1.0 g sulfonamide, 2.94 mL H_3PO_4, 0.1 g N-(1-naphthyl)-ethylenediamine dihydrochloride) and 2 mL H_2O are added one by one. After the mixed solution reacts for 10 min in the dark, the UV-Vis absorption spectra are performed at λ = 540 nm. We calibrate the standard NO_2^- solutions with different concentration and calculate the fitting curve (y=0.247x +0.0147, R^2=0.999).

Determination of N_2H_4: The electrolytes after 1 h electrolysis is diluted 20 times to 1 mL，5.99 g $C_9H_{11}NO$, 30 ml HCl and 300mL C_2H_5OH was mixed to form a uniform solution used as a color reagent. Then, 1 mL color reagent was added into electrolyte after 2 h electrolysis. The absorbance was performed at a wavelength of 455 nm after the mixture stand 20 min in dark. The fitting curve (y = 0.5718x + 0.1543, R^2 = 0.9998) shows good linear relation of absorbance value with N_2H_4 concentration.

^{15}N isotope labeling experiments: After electrolysis in 0.1 M PBS with 0.1 M $^{15}NO_3^-$ or $^{14}NO_3^-$ at –1.0 V for 24 h, the pH value of the obtained electrolyte is adjusted to be 3.0 by the addition of 0.5 M H_2SO_4 solution. Then, 1 mL of electrolyte, 0.2 mL of

DMSO and 0.2 mL of D_2O are added into the NMR tube for further NMR detection.

Computational Details:

First-principles calculations are performed by using the Vienna Ab initio Simulation Package (VASP)[1-4] to investigate the NO_3RR process on CuO and $CuFe_2O_4$ surface. The valence-core electrons interactions are treated by Projector Augmented Wave (PAW)[5] potentials and the electron exchange correlation interactions are described by the generalized gradient approximation (GGA) with the Perdew-Burke-Ernzerhof (PBE)[6] functional. Considered long-range interaction at the interface, Van der Waals interactions are considered using DFT-D3 correlation[7]. To avoid interaction come from other slabs, a vacuum of 20 Å is added along z direction. The convergence criterion of geometry relaxation is set to 0.03 eV•$Å^{-1}$ in force on each atom. The energy cutoff for plane wave-basis is set to 500 eV. The K points are sampled with 3×3×1 by Monkhorst-Pack method[8].

Gibbs free energy change (ΔG) is evaluated based on the computational hydrogen electrode (CHE) model, which takes one-half of the chemical potential of gaseous hydrogen under standard conditions as the free energy of the proton-electron pairs. ΔG is calculated by the following equation[9]:

$$\Delta G = \Delta E + \Delta E_{ZPE} - T\Delta S + neU$$

where ΔE, ΔE_{ZPE}, ΔS are the reaction energy from DFT calculation, the correction of zero-point energy and the change of simulated entropy, respectively. T is the temperature (T = 300 K). *n* and U are the number of transferred electrons and applied potential respectively.

Supplementary Figures

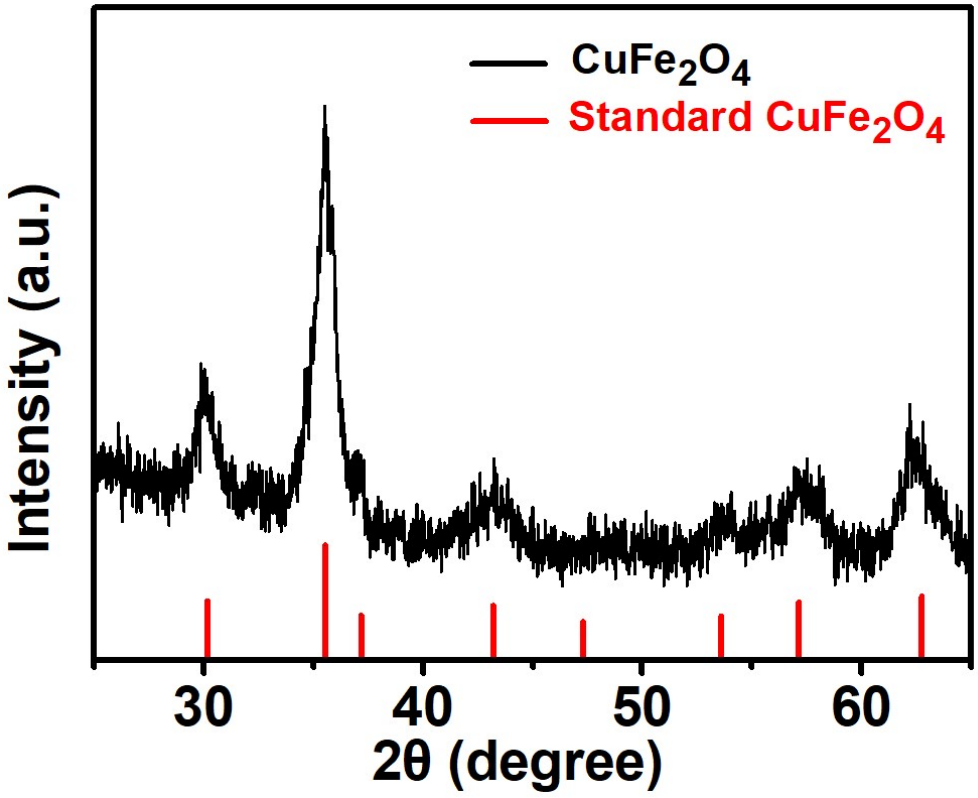

Figure S1. XRD pattern of pure $CuFe_2O_4$ fibers

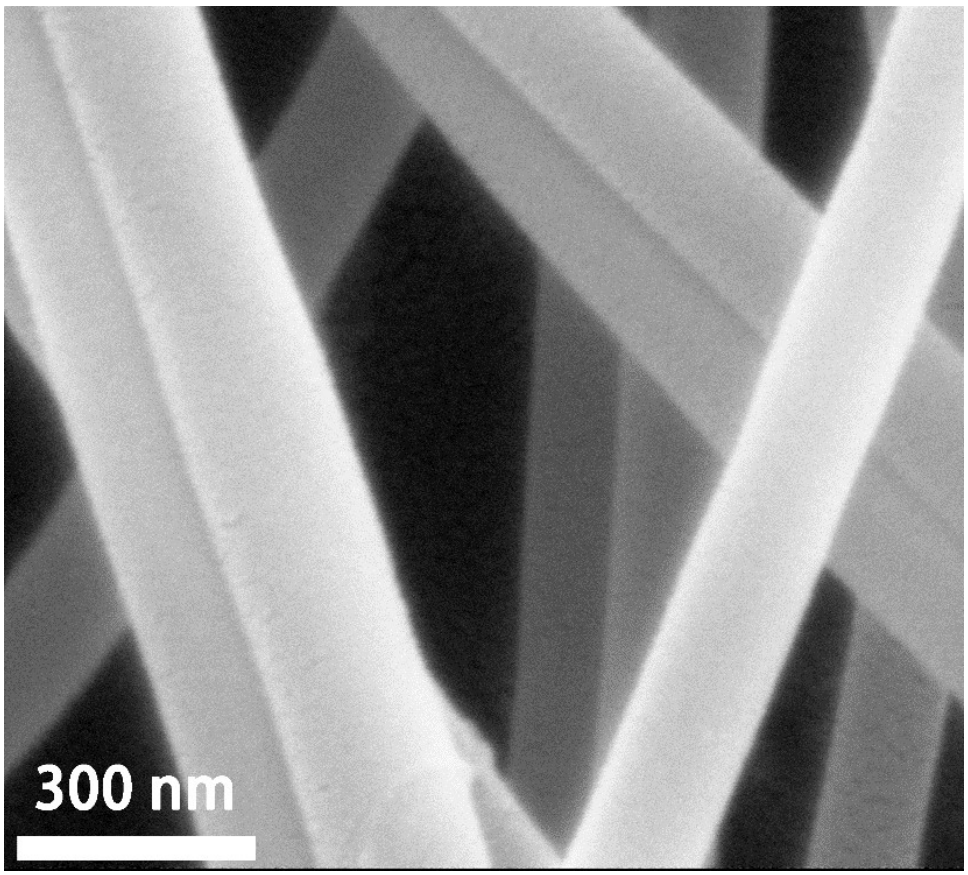

Figure S2. SEM image of CO@CFO before calcination

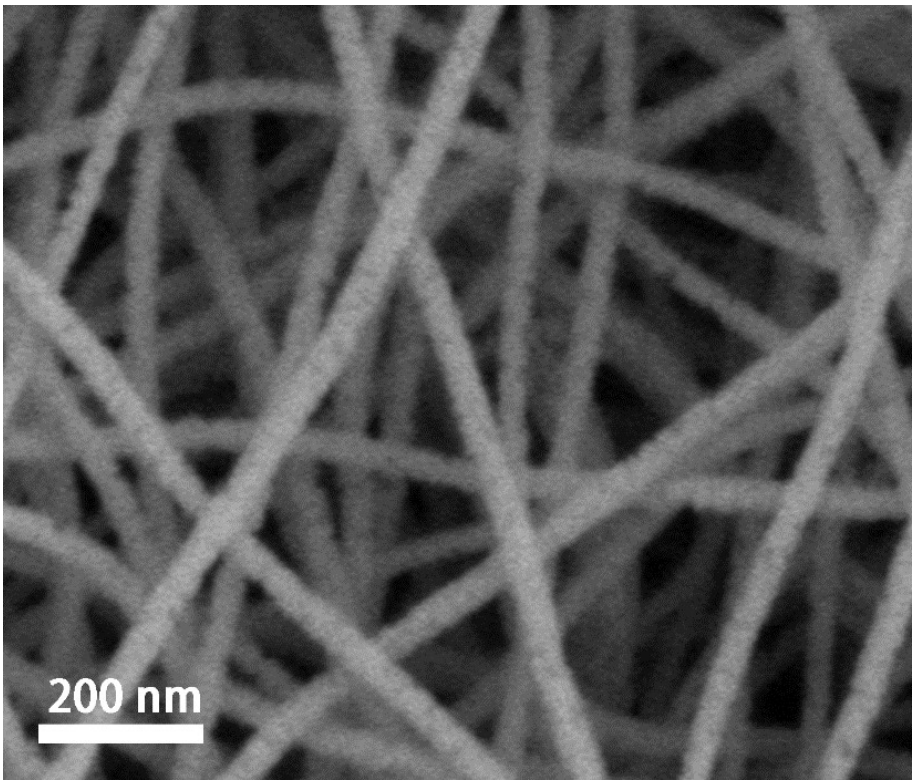

Figure S3. SEM image of pure CFO

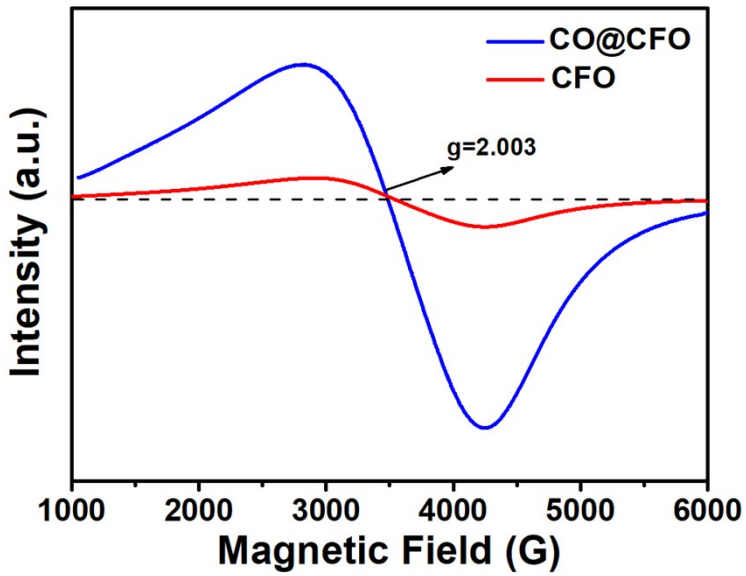

Figure S4. EPR spectra of CO@CFO and CFO.

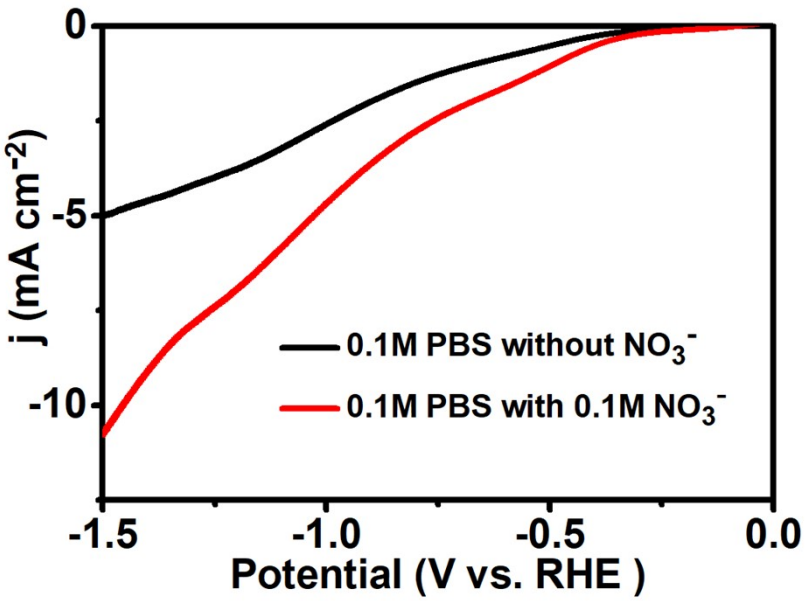

Figure S5. LSV curve of CO@CFO in 0.1M PBS electrolyte with and without NO_3^-.

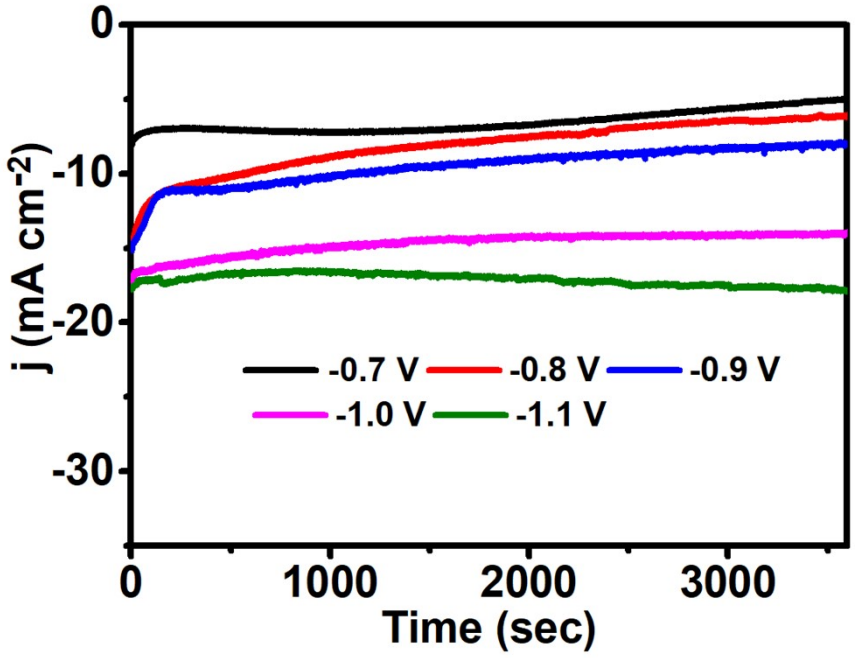

Figure S6. Time-dependent current density curves at different potentials.

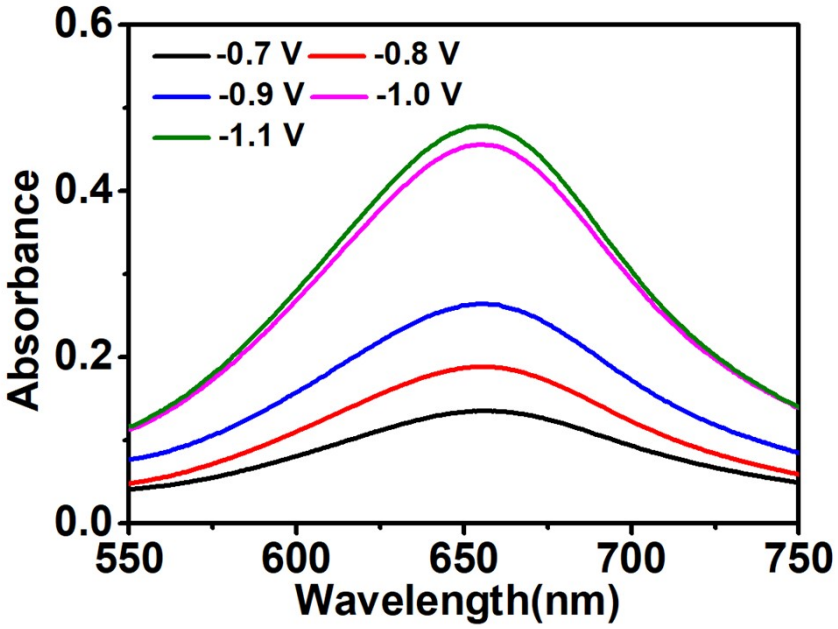

Figure S7. UV–vis absorption spectra at 5 various potentials with the indophenol indicator.

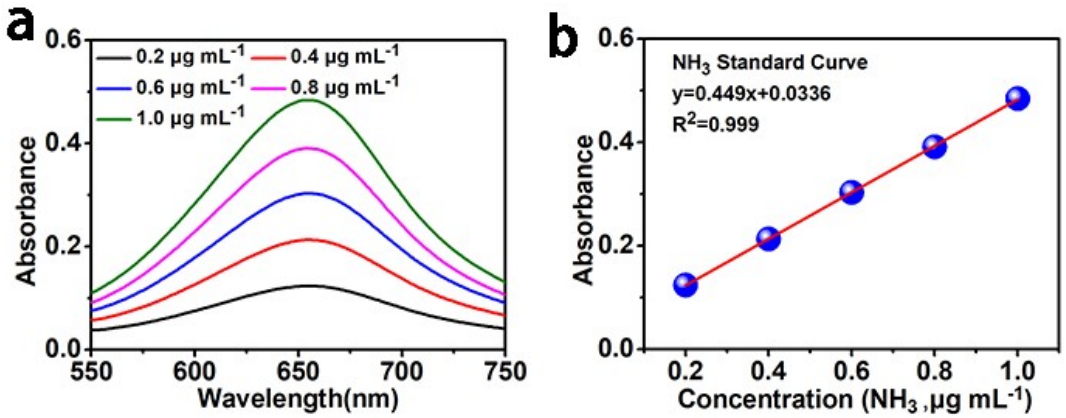

Figure S8. (a) UV-Vis absorption spectra of indophenol assays with NH_3. (b) Calibration curve used for the determination of NH_3 concentration.

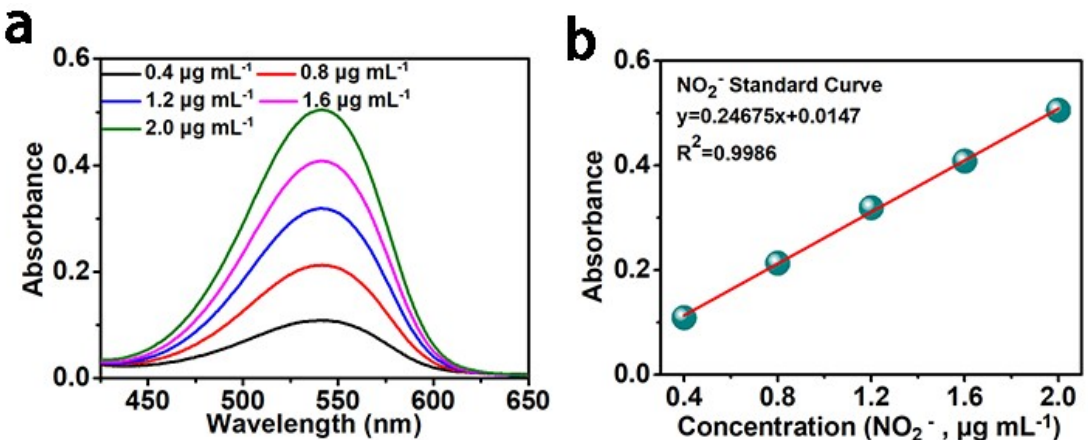

Figure S9. (a) UV-Vis absorption spectra of indophenol assays with NO_2^-. (b) Calibration curve used for the determination of NO_2^- concentration.

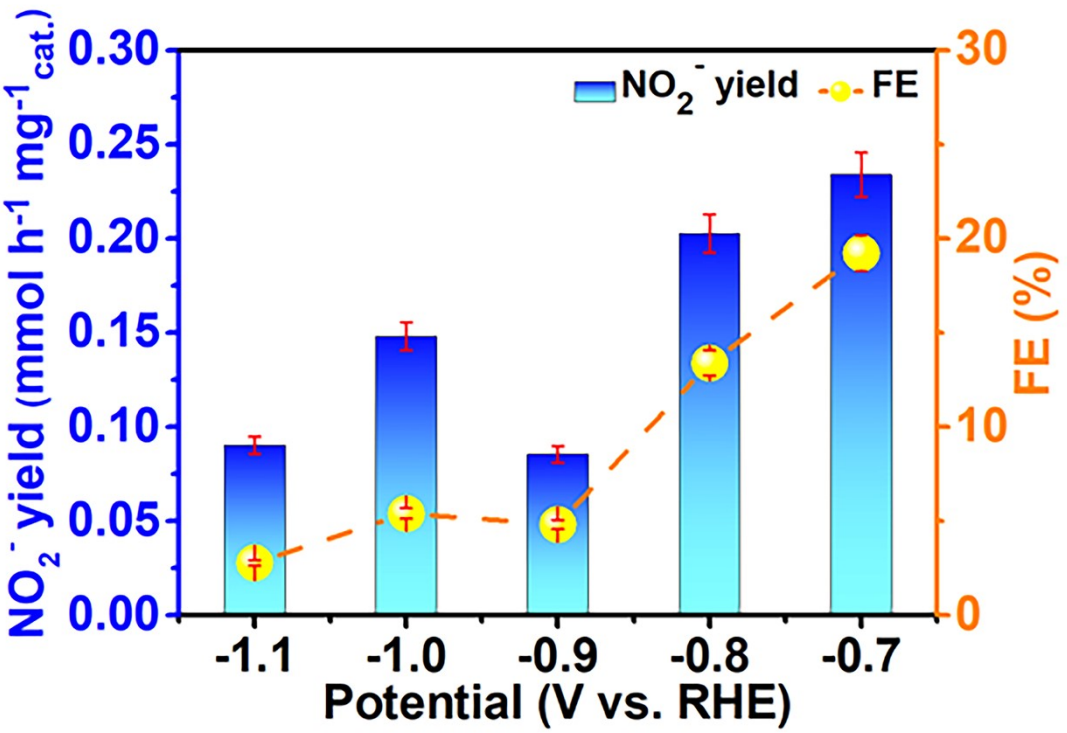

Figure S10. NO_2^- yields and FEs for CO@CFO in 0.1M PBS with 0.1M NO_3^- at different potentials

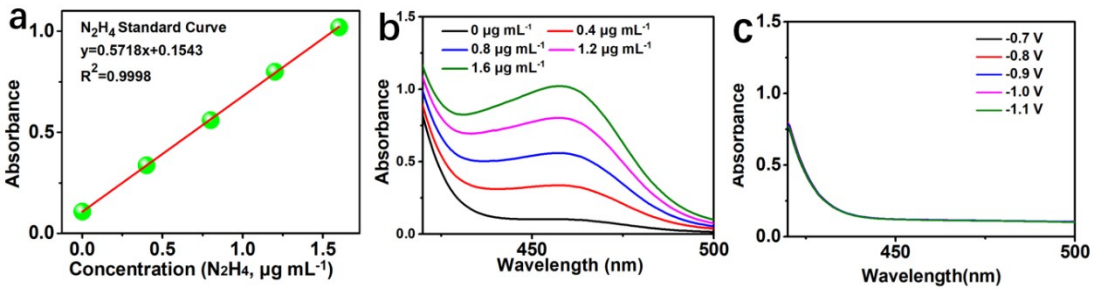

Figure S11. (a) UV-Vis absorption spectra of indophenol assays with N_2H_4. (b) Calibration curve used for the determination of N_2H_4 concentration. (c) UV–Vis absorption spectra at 5 various potentials with the indophenol indicator.

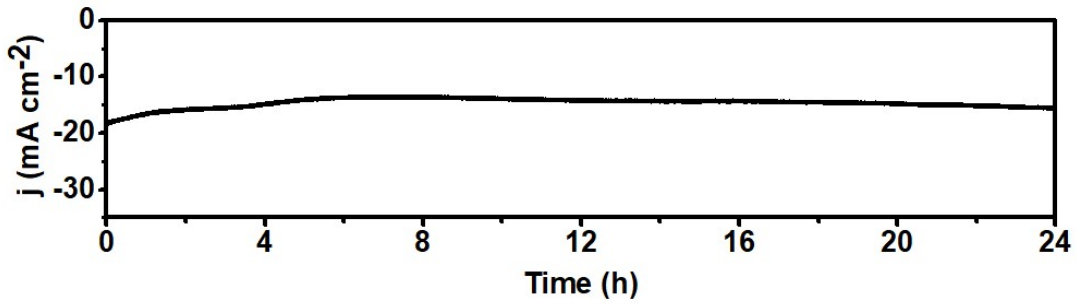

Figure S12. Time-dependent current density curves of CO@CFO at a fixed potential of −1.0 V vs. RHE for 24 h.

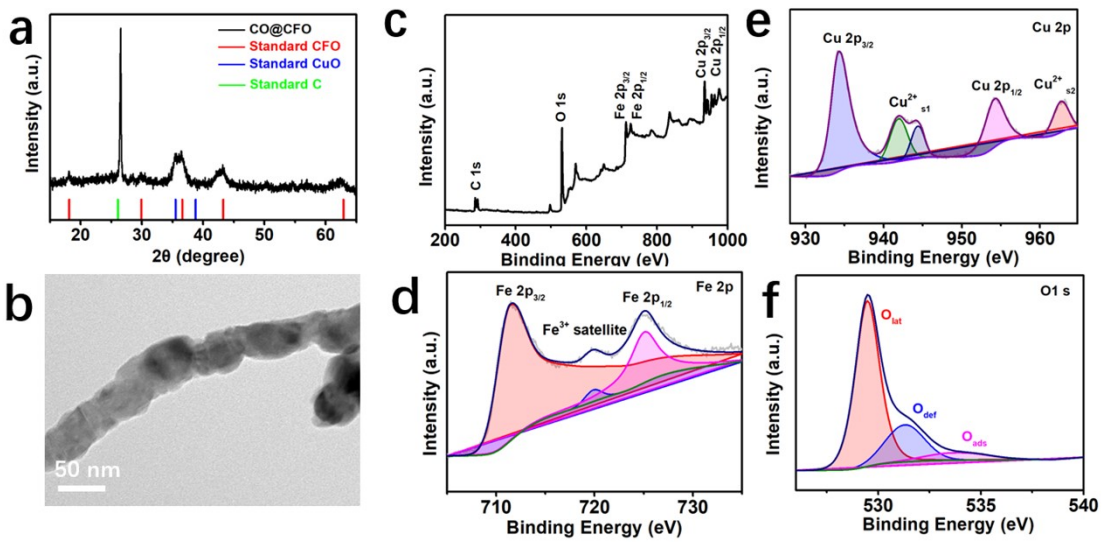

Figure S13. (a)XRD pattern, (b)TEM image, XPS(c-f) spectra for CO@CFO after 24 h electrolysis

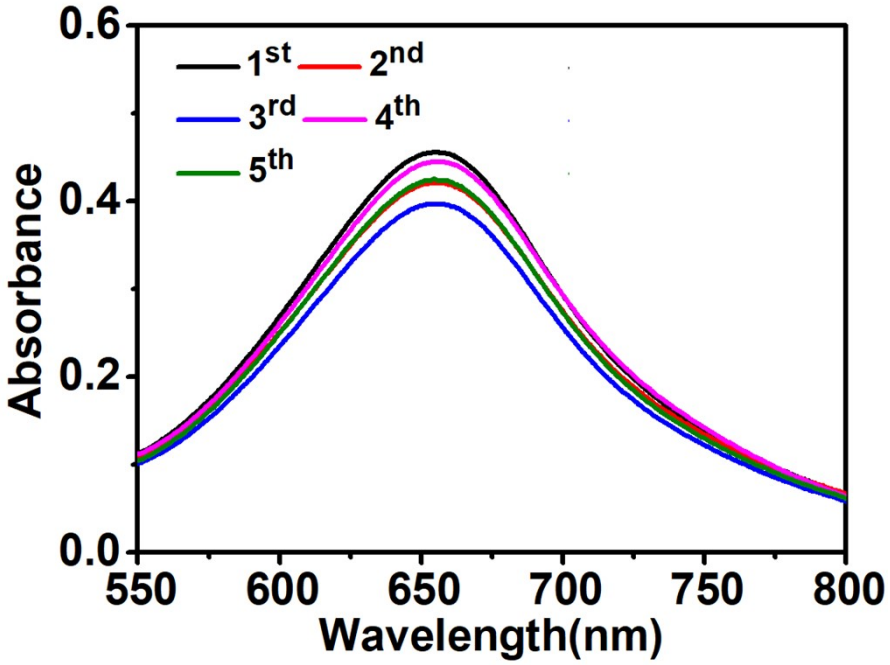

Figure S14. UV–Vis absorption spectra at identical potentials of −1.0 V vs. RHE with the indophenol indicator.

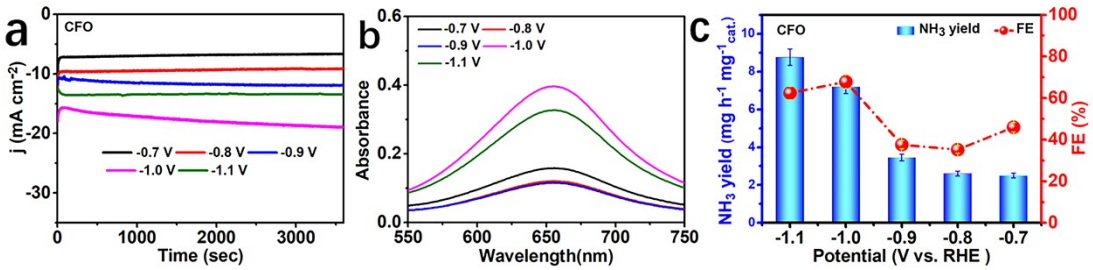

Figure S15. (a)Time-dependent current density curves at different potentials of CFO. (b) UV–Vis absorption spectra at 5 various potentials with the indophenol indicator of CFO. (c) NH_3 yields and FEs for CFO in 0.1M PBS with 0.1M NO_3^- at different potentials

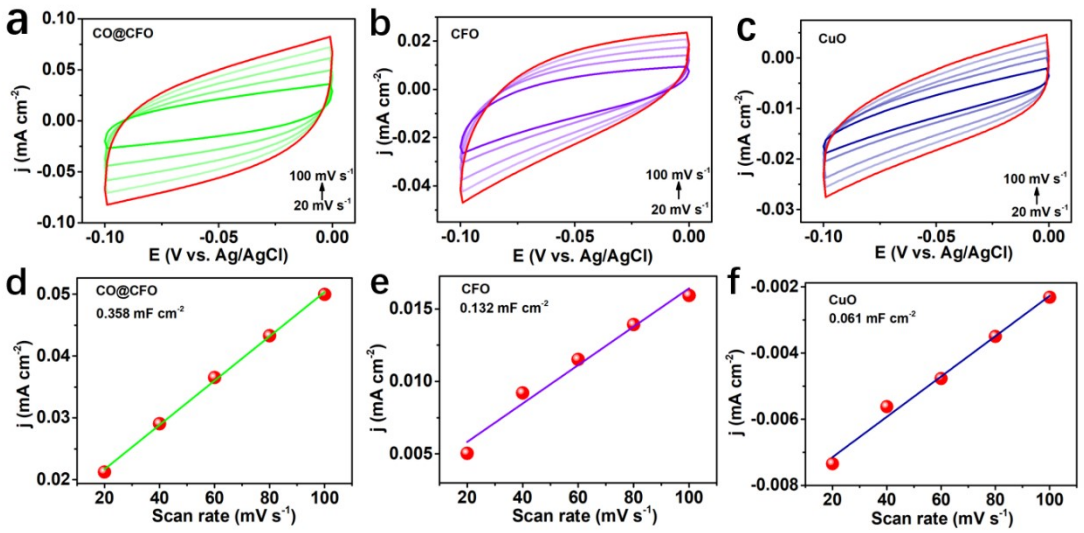

Figure S16. (a-c) CVs of CO@CFO, CFO and CuO various scan rates (20-100 mV s^{-1}) from -0.0 V to -0.10 V vs. Ag/AgCl. (d-f) Capacitive current densities at −0.05 V vs. Ag/AgCl as a function of scan rates.

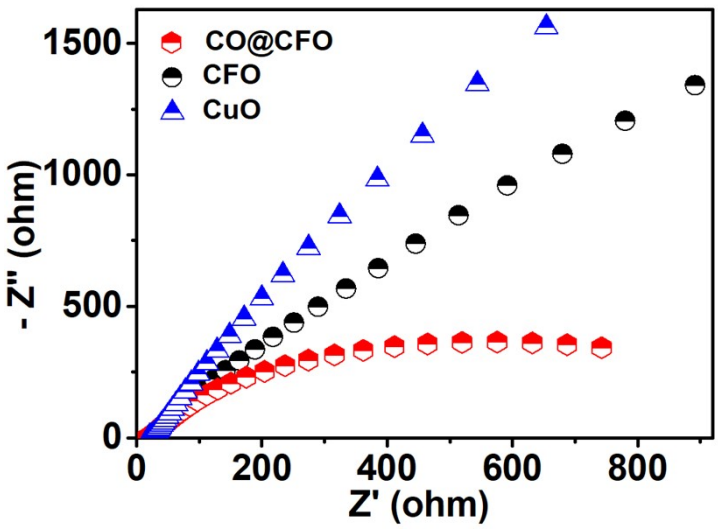

Figure S17. EIS Nyquist plots of different samples by applying an impedance amplitude of 5 mV with the frequency range from 10^{4} to 10^{-1}Hz.

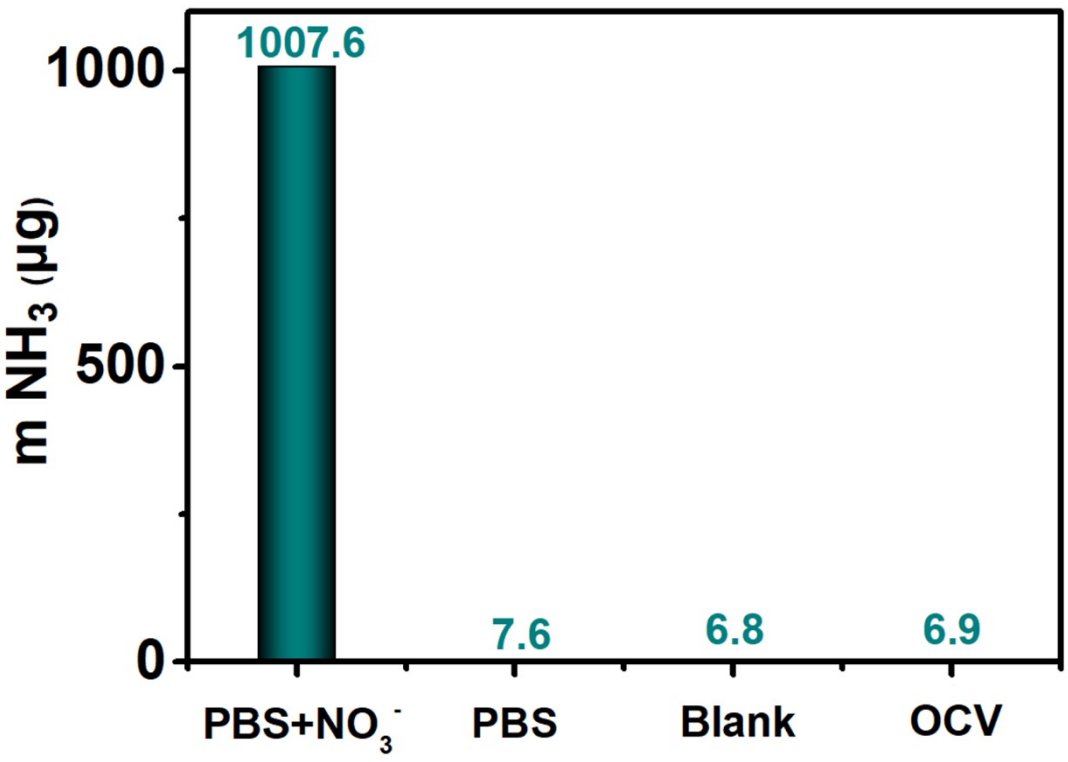

Figure S18. Comparison of amount of produced NH_3 under four different conditions.

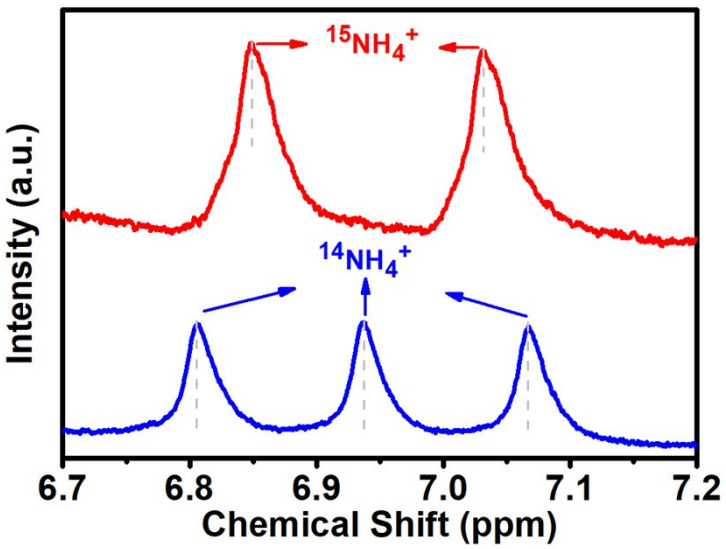

Figure S19. 1H NMR spectra of the electrolyte after electrocatalytic reaction using $15NO_3^-$ and $14NO_3^-$ as the nitrogen source.

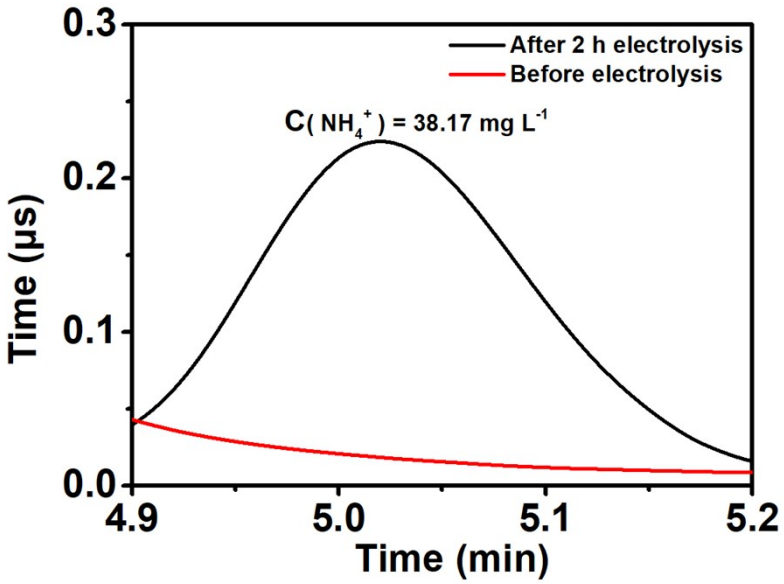

Figure S20. Ion chromatography test before and after 2 h electrolysis for CO@CFO.

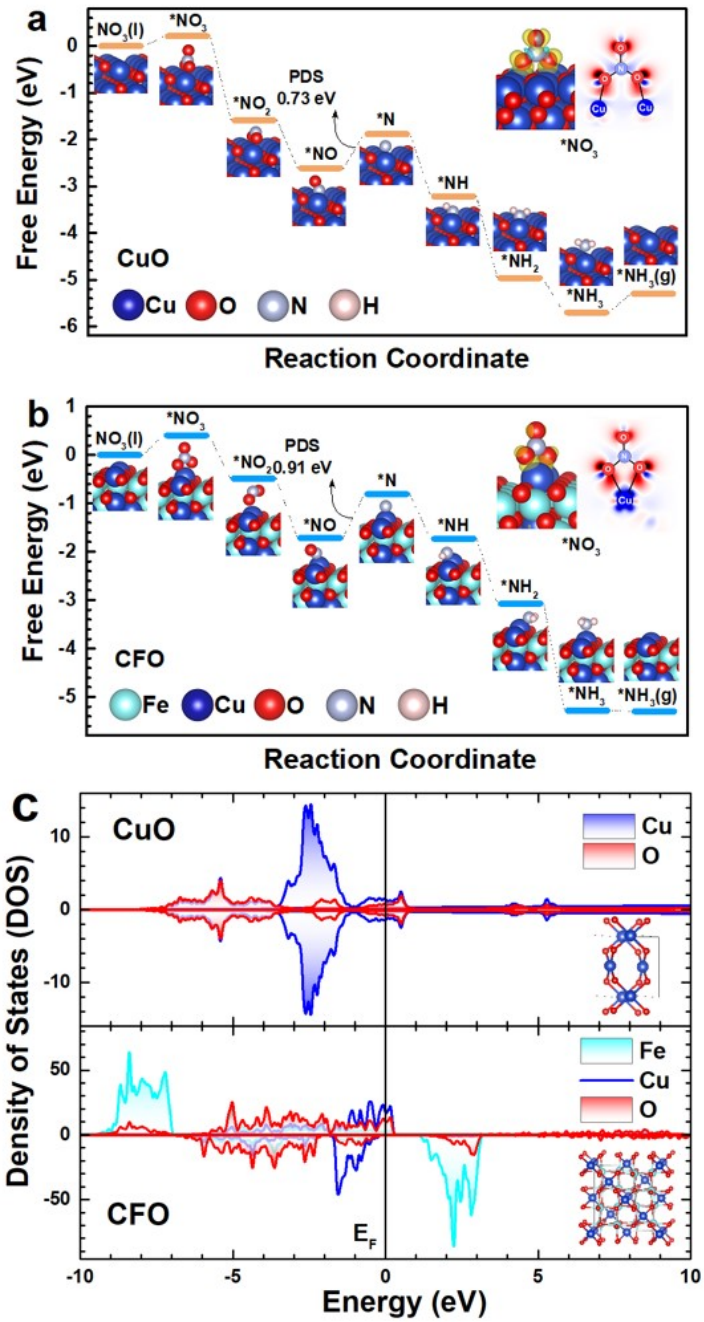

Figure S21. Calculated free energy profiles of (a) CuO and (b) CFO surfaces. The charge density difference of NO_3^- adsorption configuration is plotted in the illustration. (c) Calculated density of states of pristine CuO and CFO.

Table S1. Comparison of electrocatalytic NO_3RR performance for $CuO@CuFe_2O_4$ with other Cu or Fe-related electrocatalysts under ambient conditions.

Catalysts	Electrolyte	NH_3 yield	FE	Ref
$CuO@CuFe_2O_4$	**0.1 M PBS with 0.1 M KNO_3**	**9296.21 μg h^{-1} $mg_{cat.}^{-1}$**	**91.08%**	**This work**
CuOx nanoparticles	0.1 M KOH (50 ppm KNO_3)	449.41 ± 12.18 μg h^{-1} $mg_{cat.}^{-1}$	74.18 ± 2.27%	10
Cu/Cu_2O NWAs	0.5 M Na_2SO_4 (200 ppm NO_3^-)	4148 μg h^{-1} $mg_{cat.}^{-1}$	95.8 %	11
Cu nanosheets	0.1 M KOH (10 mM KNO_3)	390.1 μg h^{-1} mg_{cat}^{-1}	99.7%	12
NFP	0.5 M Na_2SO_4 (80 mg L^{-1} $NaNO_3$)	952 μg h^{-1} $mg_{cat.}^{-1}$	99.2%	13
TiO_2-x	0.5 M Na_2SO_4 (50 ppm NO_3^-)	765 μg h^{-1} $mg_{cat.}^{-1}$	85%	14
TiO_2	0.5 M Na_2SO_4 (50 ppm NO_3^-)	408 μg h^{-1} $mg_{cat.}^{-1}$	66.3%	14
Co3O4@NiO HNTs	0.5 M Na_2SO_4 (200 ppm NO_3^-)	117.8μg h^{-1} $mg_{cat.}^{-1}$	54.97%	15
In-S-G	-	3740 mmol $g_{cat}^{-1}h^{-1}$	75%	16
BCN@Cu	-	4609.1μg h^{-1} $mg_{cat.}^{-1}$	91.15%	17
Co_3O_4/Cu	0.4 MNa_2SO_4 (50 mg $L^{-1}NO_3^-$)	684 μg h^{-1} $mg_{cat.}^{-1}$	94.6%	18
PA-RhCu cNCs	0.1 M $HClO_4$	2400 μg h^{-1} mg_{cat}^{-1}	93.7%	19

	(0.05 M KNO_3)			

References

1. G. Kresse and J. Furthmüller, *Phys. Rev. B*, 1996, **54 (16)**, 11169.
2. G. Kresse and J. Furthmüller, *Comp. Mater. Sci.*, 1996, **6 (1)**, 15–50.
3. G. Kresse and J. Hafner, *Phys. Rev. B*, 1994, **49 (20)**, 14251.
4. M. Segall, PJ . Lindan, M J Probert, C J . Pickard, P J. Hasnip, S. Clark, M. Payne, *J. Phys-Condens Mat.*, 2002, **14 (11)**, 2717.
5. P. E. Blöchl, *Phys. Rev. B*, 1994, **50 (24)**, 17953.
6. John P. Perdew, J. A. Chevary, S. H. Vosko, Koblar A. Jackson, Mark R. Pederson, D. J. Singh, and Carlos Fiolhais, *Phys. Rev. B*, 1992, **46(11)**, 6671.
7. S. Grimme, J. Antony, S. Ehrlich and H. Krieg, *J. Chem Phys.*, 2010, **132(15)**, 154104.
8. H. J. Monkhorst and J. D. Pack, *Phys. Rev. B*, 1976, **13 (12)**, 5188.
9. Norskov J., Rossmeisl. J., Logadottir. A., Lindqvist. L., Kitchin. J., Bligaard. T. and Jonsson. H, *J. Phys. Chem. B*, 2004, **108(46)**, 17886–17892.
10. J. Geng, S. Ji, H. Xu, C. Zhao, S. Zhang and H. Zhang, *Inorg. Chem. Front.*, 2021, **8**, 5209–5213.
11. F. Lei, W. Xu, J. Yu, K. Li, J. Xie, P. Hao, G. Cui and B. Tang, *Chem. Eng. J.*, 2021, **426,** 131317.
12. XB Fu, XG Zhao, XB Hu, K. He, YN Yu, T. Li, Q. Tu, X. Qian, Q. Yue, MR Wasielewski and YJ Kang, *Appl. Mater. Today*, 2020, **19**, 100620.
13. Q. Yao, J. Chen, S. Xiao, Y. Zhang, and X. Zhou, *ACS Applied Materials & Interfaces*, 2021, **13 (26)**, 30458–30467.
14. R. Jia, Y. Wang, C. Wang, Y. Ling, Y. Yu, and B. Zhang, *ACS Catalysis*, 2020, **10 (6)**, 3533–3540.
15. Wang, Y., Liu, C., Zhang, B. et al., *Sci. China Mater.,* 2020, **63**, 2530–2538.
16. Fengcai Lei, Wenli Xu, Jing Yu, Kun Li, Junfeng Xie, Pin Hao, Guanwei Cui, Bo Tang, *Chemical Engineering Journal,* 2021, **426**,131317.
17. X. Zhao, G. Hu, F. Tan, S. Zhang, X. Wang, X. Hu, A.V. Kuklin, G.V. Baryshnik ov, H. Ågren, X. Zhou, H. Zhang, *J. Mater. Chem. A*, 2021, **9 (41)**, 23675–23686.

18. W. Fu, Z. Hu, Y. Du, P. Su, Y. Su, Q. Zhang, M. Zhou, *Journal of Hazardous Materials*, 2022, **434**, 128887.
19. Z. Ge, T. Wang, Y. Ding, S. Yin, F. Li, P. Chen, and Y. Chen, *Adv. Energy Mater.* 2022, **12**, 2103916.